Wear 460–461 (2020) 203461

Contents lists available at ScienceDirect

Wear

journal homepage: http://www.elsevier.com/locate/wear

Wear of electroplated diamond tools in lap-grinding of Al_2O_3 ceramic materials

Mariusz Deja *, Dawid Zieliński

Gdańsk University of Technology, Faculty of Mechanical Engineering, Department of Manufacturing and Production Engineering, 11/12 G. Narutowicza Str., Gdańsk, PL 80-233, Poland

ARTICLE INFO

Keywords:
Abrasive finishing
Diamond grains
Electroplating
Tool wear
Ceramic samples
Empirical model

ABSTRACT

Current development of modern products, together with ever-increasing demands for their operation and usage, necessitate the search for new processing methods. Abrasive machining is widely used in many industrial areas, especially for processing difficult-to-machine materials such as advanced ceramics. Grinding with lapping kinematics, also called lap-grinding, is still one of the innovative methods of abrasive processing being under continuous development. It combines the advantages of grinding and lapping, allowing for meeting high design requirements and, at the same time, ensuring efficient and safe machining. This paper presents experimental and modelling results on the application of electroplated wheels with diamond grains (D107 and D64) in the lap-grinding of Al_2O_3 ceramic materials in a single-disc lapping machine configuration. The grain size along with the thickness of the nickel bond influenced the material removal rate and surface roughness obtained. The relationship between the material removal and the processing time was approximated by asymptotic mathematical functions. Moreover, the empirical models were modified according to the Preston's equation when the unit pressure increased. The linear and nonlinear regression models enabled accurate curve fitting to the surface roughness data. Microscopic images of the active surface of electroplated diamond tools were analyzed in the aspects of the resultant tool wear and technological effects. In addition, the results were referred to the analysis of microscopic images of the suspension taken from the active surface of the tool after subsequent tests. The suspension consisted of particles of fragmented abrasive grains as well as chips removed from the machined surface.

1. Introduction

The selection of an appropriate finishing method for a specific application depends on many factors, such as: the size and shape of the workpiece, way of fixturing, production rate and the range of acceptable shape errors. Grinding and lapping are the basic manufacturing techniques used for obtaining fine surface finish along with high dimensional and shape accuracy, by reduction of surface roughness and precise removal of material [1]. A wide spectrum of unique advantages of some materials, especially advanced ceramics, poses serious challenges and difficulties in choosing the suitable method for their machining. Due to corrosion resistance and high mechanical properties, a wide variety of mechanical components, e.g., for automotive and aerospace industry, as well as cutting tools for machining of heat resistant superalloys are made of ceramics of different grades [2]. Alumina, zirconia and silicon carbide-based ceramics have the highest application potential [3]. Aluminum oxide (Al_2O_3) ceramics, examined in this paper, is known as a very difficult to machine material with superior properties such as high hardness and strength at elevated temperatures as well as high wear resistance [4]. Poser et al. showed in Ref. [5] the potential of oxide ceramics reinforced or modified by second phases as friction materials. Embedding TiN particles into the surface of commercially available Al_2O_3 ceramic using a laser-assisted process substantially improved stability of a friction coefficient compared with the monolithic alumina used for reference. Laser-assisted machining (LAM) can be used for manufacturing precision aluminum oxide ceramic parts with increased material removal rate (MRR) and much better workpiece surface quality in comparison with conventional machining [6]. Diamond grinding is often the method of choice in machining ceramic pars [7] but the subsurface damage and crack formation tendency is related to the high hardness and brittleness of ceramic materials [8]. A high tendency for brittle cracking during abrasive machining leads to surface defects and

* Corresponding author.
E-mail addresses: mariusz.deja@pg.edu.pl (M. Deja), dawid.zielinski@pg.edu.pl (D. Zieliński).

https://doi.org/10.1016/j.wear.2020.203461
Received 20 April 2020; Received in revised form 28 July 2020; Accepted 26 August 2020
Available online 29 August 2020

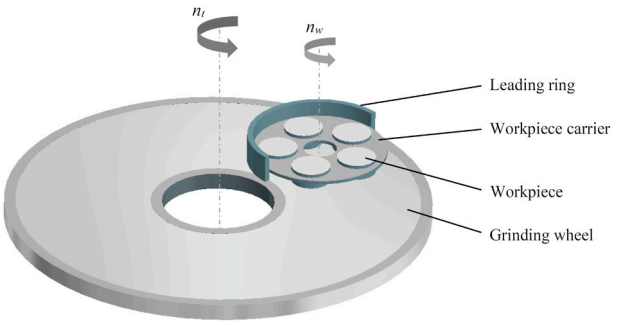

Fig. 1. Schematic drawing of single-disc grinding with lapping kinematics, including the main components of the machine tool as well as main kinematical process parameters, i.e., the rotational velocity of a tool (n_t) and leading ring (n_w).

deterioration of the strength and functional properties of manufactured parts. In addition, high temperature generated in the machining zone during grinding, resulting from the interaction between the grinding wheel and the workpiece, may lead to the formation of burns, as well as microstructural transformations in the subsurface layers [9]. The tool marks, surface waviness or subsurface damage resulting from preceding processing can be effectively reduced or even removed by different manufacturing techniques, such as fine [10] or single-pass grinding [11], chemical mechanical polishing (CMP) [12] and lapping [13]. Shibata et al. [14] used a fast Fourier transform (FFT) method for the comprehensive analysis of surface profiles characteristics obtained during lapping, correlated with shape information of grit particles within narrow size ranges. Deshpane et al. showed in Ref. [15] that the use of different abrasives affects surface roughness and topography more than the material removal rate. Harder grits allowed obtaining the better surface finish and flatness. Besides, the type and quantity of lubricant influence the surface finish and the process efficiency are investigated. The minimum quantity lubrication (MQL) can reduce the surface and sub-surface damages as reported in Ref. [16] for high-speed grinding (HSG) of engineering ceramics. Emami et al. [17] successfully utilized ecological safe MQL oils in Al_2O_3 ceramic grinding, and studied the influence of base oil and additive type on grinding force and surface roughness.

Numerous research works focus on the use of high-speed [18] or super high-speed grinding [19] for ceramic materials, characterized by an increased peripheral speed of the grinding wheel, about 2–3 times higher than in conventional grinding. Increasing the peripheral speed of the grinding wheel allows attaining high productivity with minimal surface damage to brittle materials [20]. In lapping, the cutting speeds are approximately 10 times lower than in grinding which results in lower heat generated during machining and, as a consequence, subsurface damage can be avoided. The removal of a relatively small amount of the workpiece material is carried out by loose abrasive micrograins suspended in oil or water slurry [21]. Lapping, as the basic flattening process, is used to obtain a high degree of flatness of a single surface (single-sided lapping) [22] or parallelism between two machined surfaces (double-sided lapping) [23].

Increasing demands from the industrial sector require the search for new and more efficient abrasive machining methods and tools. Trends presented by Oliveira et al. in Ref. [24] refer to the automotive industry, as a particularly important sector for abrasive machining. Grinding with lapping kinematics was pointed out as one of the main industrial challenges and directions of the abrasive machining development. This type of machining, also often referred to as lap-grinding [25], combines the advantages of both processes: high grinding efficiency and a high degree of flatness obtained by lapping [26]. A characteristic feature of grinding with lapping kinematics consists in the use of grinding wheels or special discs covered with an abrasive layer, as a replacement for standard lapping discs [27]. Grinding with lapping kinematics, in contrast to conventional lapping, is a faster and cleaner material removal process as shown for sapphire wafers in Ref. [28] and for oxide ceramics in Ref. [29].

In lap-grinding, the combination of the aforementioned grinding and lapping characteristic features enables the achievement of high dimensional and shape accuracy, as well as low roughness of the machined surfaces, while increasing process efficiency [30]. Kim et al. [31] compared two-body and three-body lapping systems for sapphire substrates, showing higher removal rates and surface roughness for a fixed diamond abrasive pad (two-body removal process). One of the main challenges related to the economic aspects of a single-sided [32] and double-sided lap-grinding [33] is the reduction of the tool wear which is usually not uniform along the tool radius due to the process kinematics [34].

Taking into account the abovementioned factors and trends in the development of contemporary abrasive processes, it can be stated that conventional lapping is being increasingly replaced by lap-grinding. Double-sided kinematical configuration is suitable for conventional [35] or high speed machining [29] and a single-sided one for processing with lower cutting speeds, typical for lapping [36].

The surface finishing with the roughness parameter Ra = 0.08 nm and the flatness deviation of 0.4 μm indicated a very high potential of single-sided lap-grinding and the pertinence of conducting further research on its development for wider industrial application [37]. As presented in Ref. [38] single-sided lap-grinding with the electroplated tools can be carried out in a standard machine configuration with freely driven conditioning rings as well as in a modified kinematical system with independently driven rings. In general, electroplated tools are characterized by high versatility of their application. The obtained structure with characteristic large free spaces between abrasive grains determines the free removal of chips during machining, as well as the proper delivery of coolant to the working zone [39]. A characteristic feature of electroplated grinding wheels is the capability to cover tool bodies of any shape with an abrasive layer although tool life is a crucial factor to be determined for single-layer electroplated diamond [40] or cubic boron nitride (cBN) tools [41]. For cost-effective application of plated wheels, it is necessary to estimate the grinding performance and to know when to replace the wheel [42]. The phenomena of the wear of electroplated cBN wheels during grinding internal cylindrical and straight surfaces was presented by Shi & Malkin in Ref. [43]. The effect of cBN grain hardness and the height of the nickel plating on the wear of the active surface of the grinding wheel and on the workpiece surface quality were studied in Ref. [44]. The technological effects after single-sided lap-grinding with the use of diamond and cBN electroplated tools were demonstrated by Deja in Ref. [45,46], respectively. It was also shown that the process kinematics [47] and the plating thickness [45] had a considerable influence on the tool wear and consistently on the removal rate as well as surface finish obtained [48].

Targeting widening the applicability of electroplating tools as well as increasing the machinability of ceramics, the objective of this research is to show a potential and limitations of single-sided lap-grinding. The paper presents experimental and modelling results on the application of diamond electroplated wheels in lap-grinding of Al_2O_3 ceramic materials. The grain size along with the thickness of the nickel bond influenced the material removal rate and the obtained surface roughness. Empirical models proposed by authors can be used for calculating the material removal and the surface roughness during lap-grinding of ceramic materials. The coefficients of asymptotic mathematical formulas of developed models gave the direct information about the expected tool life. Moreover, the empirical models were modified according to the Preston's equation when the unit pressure increased. The recommendations for selecting a model for predicting material removal, depending on the plating thickness, were given. Furthermore, microscopic images of different areas of the active surface of electroplated diamond tools were analyzed in the aspects of the resultant tool

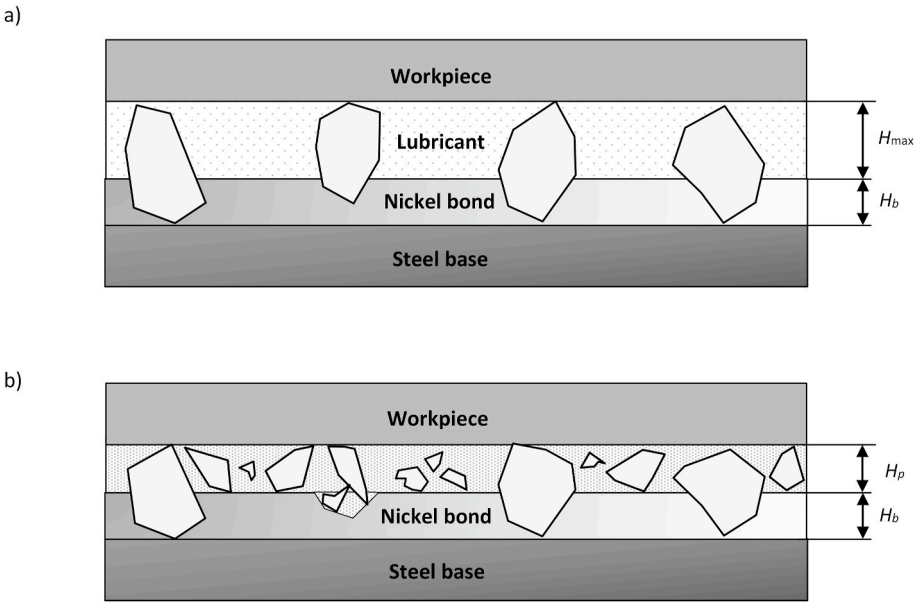

Fig. 2. Electroplated tool at the beginning of the lap-grinding process with the maximum height of grain exposure H_{max} (a) and after processing time t_p with the reduced grain exposure H_p (b).

Table 1
Process conditions during lap-grinding experiments.

Lapping disc		
Outer tool diameter	d_o	380 mm
Inner tool diameter	d_i	90 mm
Grain material		Diamond (D)
Grain size	d_g	64 μm
		107 μm
Areal concentration of grains	C_{64}	130 mm^{-2}
	C_{107}	70 mm^{-2}
Bond type		Nickel
Bond thickness to grain size ratio	T_b	35%
		50%
		65%
Lapping parameters		
Rotational speed of a lapping plate	n_t	60 min^{-1}
Rotational speed of a leading ring	n_w	121 min^{-1}
Duration of a single test	t_t	90 s
Unit pressure	p_1 for $t_p \leq 540$ s	10 kPa
	p_2 for $t_p > 540$ s	14 kPa
Lubricant		
Machining oil		
Kinematic viscosity at temp. 40 °C	N	10.5 mm^2 s^{-1}
pH		5.60
Flow rate	$\bar{Q}_{lub}$	3 ml/min
Workpiece properties		
Material		Al_2O_3
Vickers hardness	HV10	1100 MPa
Diameter	d_w	34 mm
Initial height	h_{w0}	20 mm
Initial surface roughness	Ra	1.8 μm

wear and technological effects. In addition, obtained results were referred to the analysis of microscopic images of the suspension taken from the active surface of the tool after each subsequent test.

2. Experiment setup and investigations

Fig. 1 presents a schematic drawing of the analyzed lap-grinding process together with a description of the major construction elements of a machine tool. The required unit pressure was achieved by adjusting the compression spring placed inside the leading ring and acting on the workpieces. In addition, there was no contact between the leading ring and the tool, which significantly reduced the tool wear. Only machined surfaces were in contact with the tool active surface through the constituted abrasive slurry. The slurry consisted of lubricant, particles of fractured grains, and chips of ceramic material removed from the machined surface.

Electroplated wheels with the nickel bond and diamond grains D107 and D64 (size distribution and dimensional range according to ISO 6106–2005) were used in the presented research. Grinding wheels of this type are constructed in such a way that the abrasive grains are immersed in a layer of bond (usually nickel) which is applied to a steel body. As seen in Fig. 2 a, the initial crystal exposure H_{max} depends on the thickness of the nickel bond layer H_b as well as on the average grain size d_g assumed as 107 μm and 64 μm for diamond grains D107 and D64, respectively. The bond thickness to the grain size ratio was calculated using the formula:

$$T_b = (H_b / d_g) \cdot 100\% \quad (1)$$

where: T_b – plating ratio in %, H_b - bond thickness in μm, d_g – average grain size in μm.

Similarly as in Ref. [44], the nickel plating with an appropriate thickness was made according to three values of the T_b ratio corresponding to 35%, 50% and 65% of the nominal diamond crystal size. The areal packing density of abrasive grains on the unused wheel surface measured from microscopic images was 130 mm^{-2} (±15 mm^{-2}) and 70 mm^{-2} (±7 mm^{-2}) for diamond grains D64 and D107, respectively. As seen in Fig. 2 b, grain fracturing resulted in reduced grain exposure H_p as well as in progressive increase in the active grain density after processing time t_p.

Detailed information on the process conditions used during lap-grinding experiments, including characteristics of grinding wheels, lubricant and cylindrical aluminum oxide Al_2O_3 ceramic samples is presented in Table 1. The pH of the lubricant was determined using a pH-meter (Mettler Toledo Seven Easy model) after preparing its aqueous solution. For this purpose, 25 cm^3 of oil was mixed with 25 cm^3 of distilled water for 15 min. After the phase separation, the pH of the aqueous layer was measured three times. The contribution of the slightly acidic conditions of conducted experiments to material removal was not examined as it was constant during all tests. However, Nowak & Kalin emphasized in Refs. [49] that for alumina, high wear occurred at very high and very low pH values of aqueous solution. Gant & Gee showed in

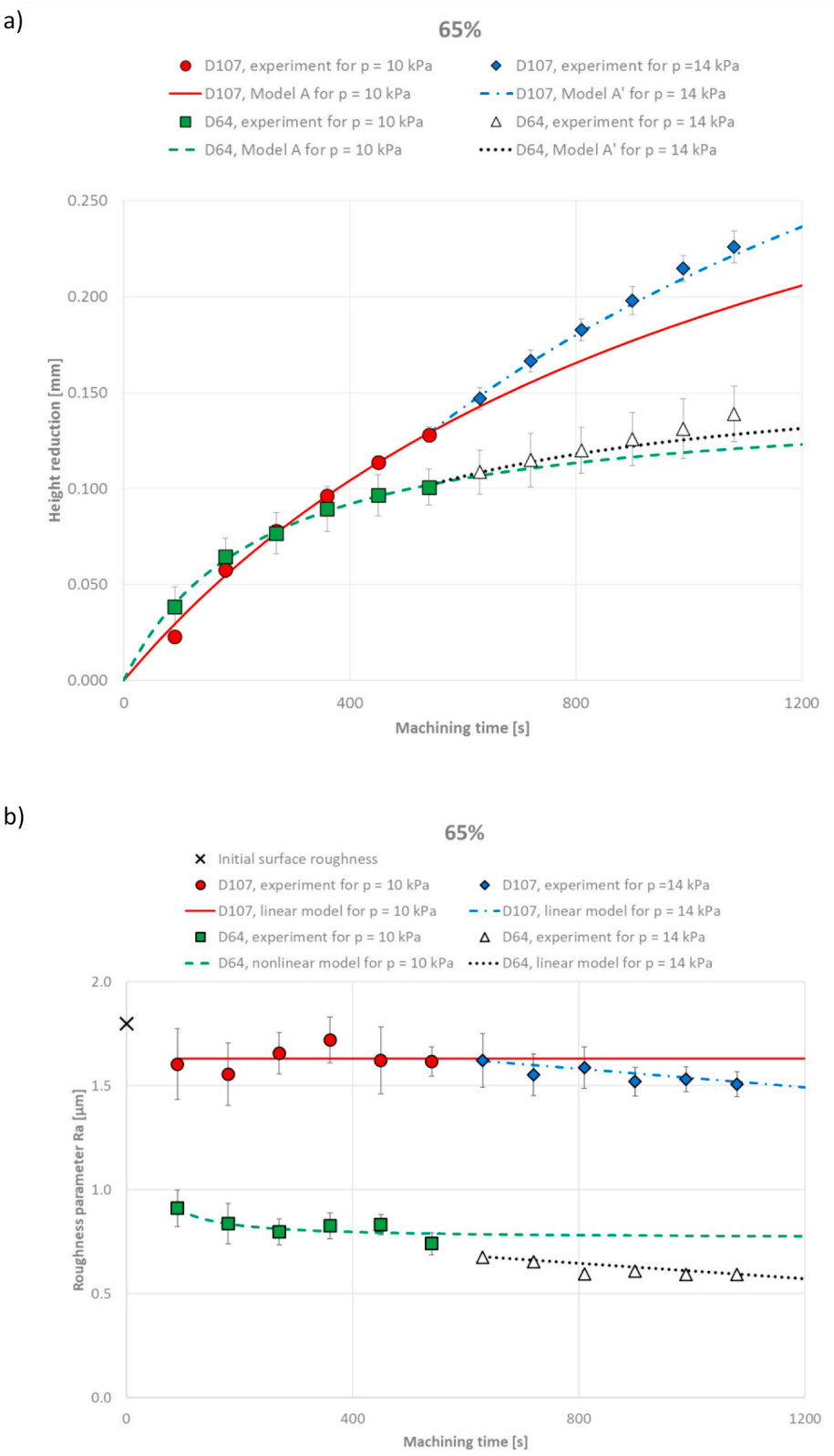

Fig. 3. Technological effects of lap-grinding of Al_2O_3 ceramics using a diamond electroplated tool with the plating thickness corresponding to 65% of a nominal diamond crystal size: experimental and theoretical material removal (a) and surface roughness (b); see Table 1 for process parameters.

Ref. [50] that alumina ceramics exhibited increasing wear with decreasing pH. This might suggest a slightly more positive than negative influence of the applied lubricant with a measured pH value of 5.6 on the material removal during lap-grinding experiments.

The height measurement was performed using a Mitutoyo micrometer with a resolution of 0.001 mm while surface roughness was measured using a contact profiler HOMMEL TESTER T500 in compliance with DIN4777 standards. A total of nine measurements of each type, at three selected places on three samples, were made after each test. The standard deviation of measured data was shown as error bars in

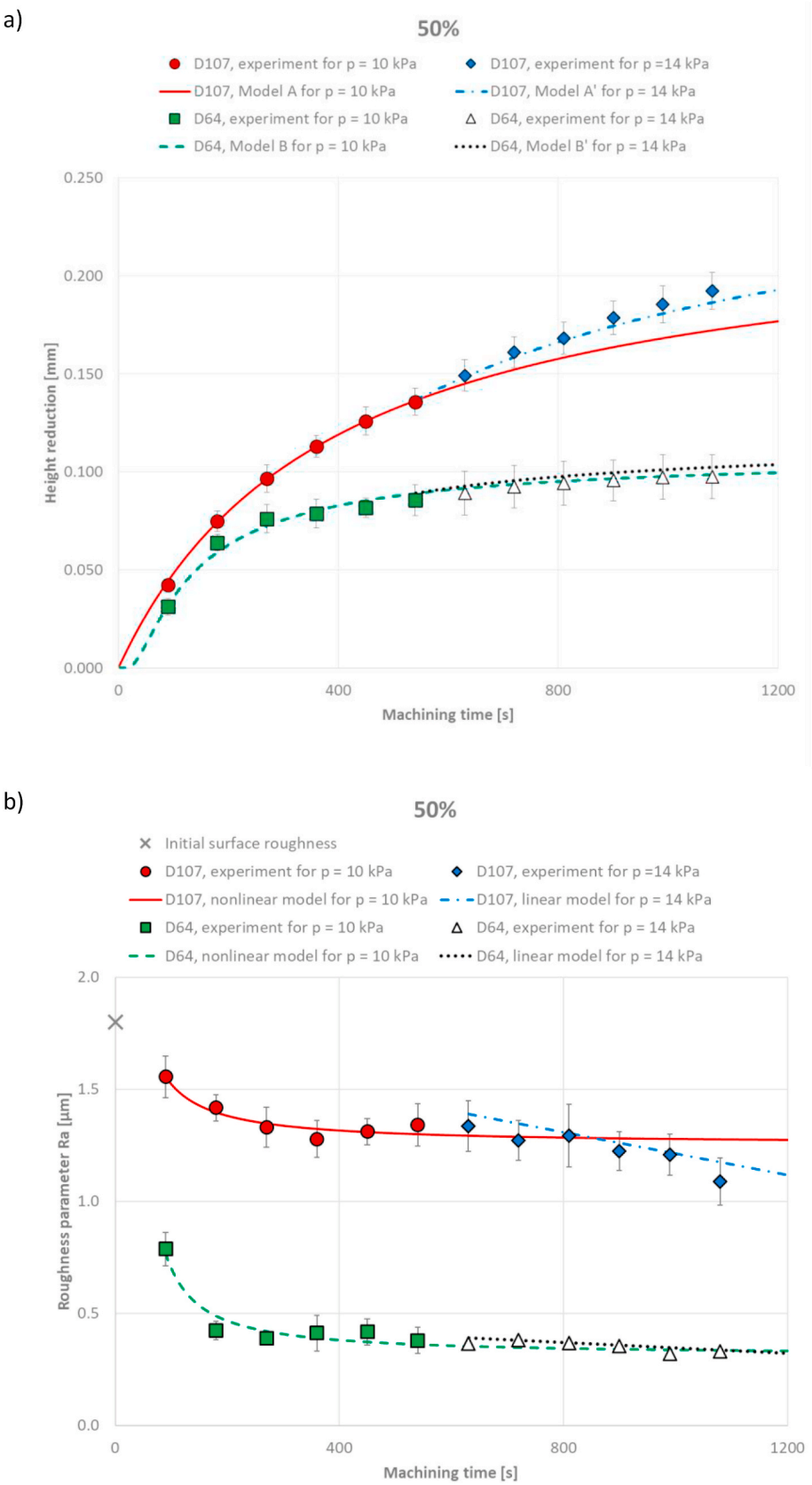

Fig. 4. Technological effects of lap-grinding of Al_2O_3 ceramics using a diamond electroplated tool with the plating thickness corresponding to 50% of a nominal diamond crystal size: experimental and theoretical material removal (a) and surface roughness (b); see Table 1 for process parameters.

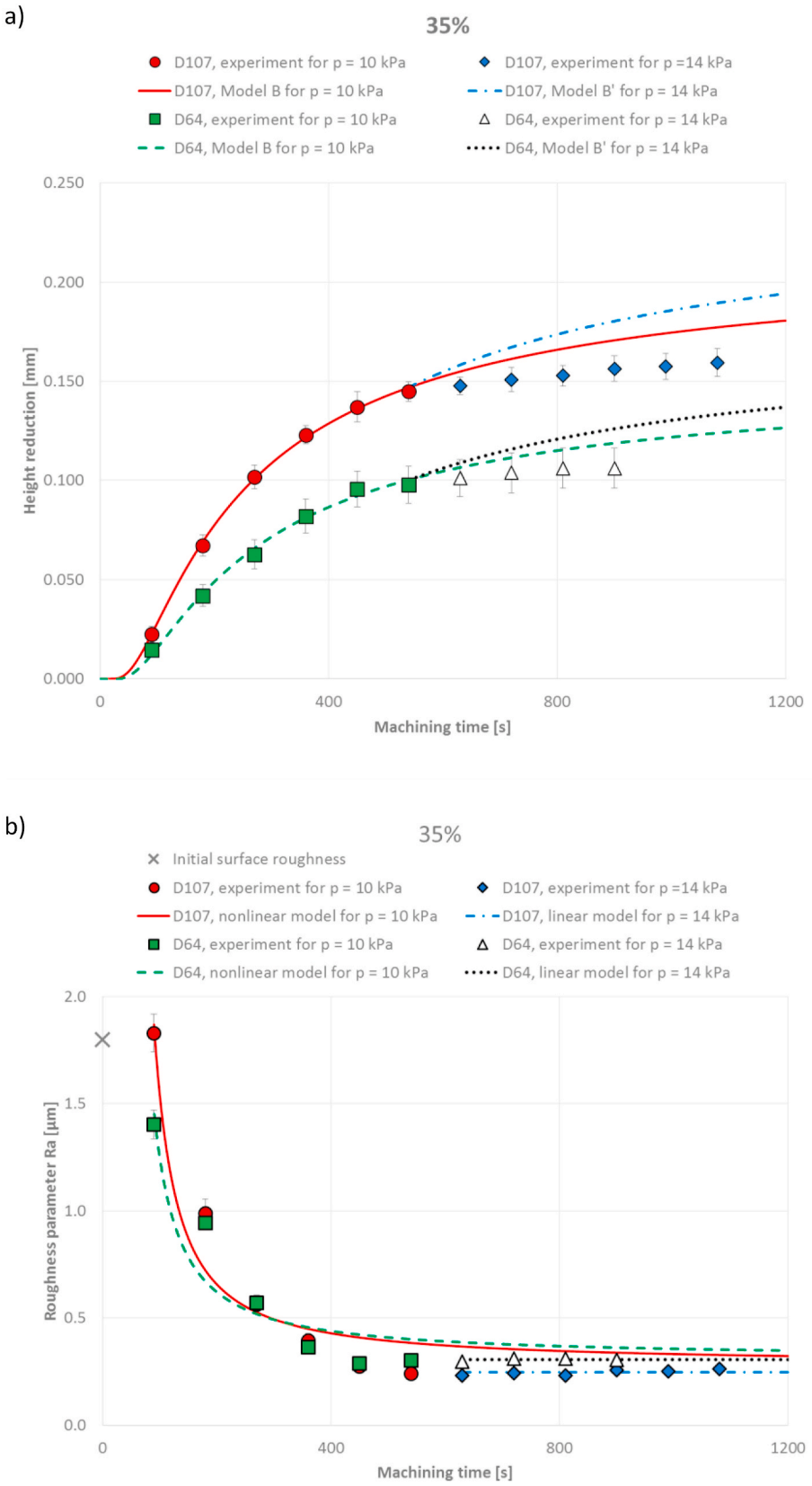

Fig. 5. Technological effects of lap-grinding of Al_2O_3 ceramics using a diamond electroplated tool with the plating thickness corresponding to 35% of a nominal diamond crystal size: experimental and theoretical material removal (a) and surface roughness (b); see Table 1 for process parameters.

Table 2
Parameters of the analyzed models for predicting the material removal in lap-grinding during processing time $0 < t_p \leq 540$ s; see Table 1 for process parameters.

Grain size	T_b ratio	Model	Coefficient	Coefficient	Horizontal asymptote	RMSE
		*) selected	b_1	b_2	y	
D107	65%	A*	3.5149e-04	8.7413e-04	0.4021	0.0033
		B	0.1807	−209.7014	0.1807	0.0043
	50%	A*	6.0714e-04	0.0026	0.2337	0.0007
		B	0.1692	−137.6934	0.1692	0.0042
	35%	A	4.6271e-04	0.0012	0.3871	0.0078
		B*	0.2139	−203.2105	0.2139	0.0014
D64	65%	A*	6.0623e-04	0.0041	0.1485	0.0014
		B	0.1218	−110.6385	0.1218	0.0021
	50%	A	5.6412e-04	0.0044	0.1297	0.0038
		B*	0.1093	−110.9386	0.1093	0.0023
	35%	A	2.7710e-04	8.1054e-04	0.3419	0.0051
		B*	0.1529	−227.8611	0.1529	0.0025

Table 3
Parameters of the selected models for predicting a surface roughness parameter Ra in lap-grinding under the unit pressure $p_1 = 10$ kPa and $p_2 = 14$ kPa; see Table 1 for process parameters.

Grain size	T_b ratio	Unit	Selected	Coefficient b_1	Coefficient	RMSE
		pressure	model	(an asymptote y for nonlinear model N)	b_2	
D107	65%	p_1	L	1.6293	–	0.0504
		p_2	L	1.7441	−2.2254e-04	0.0205
	50%	p_1	N	1.2539	19.451	0.0272
		p_2	L	1.6456	−4.7746e-04	0.0290
	35%	p_1	N	0.2793	171.11	0.1385
		p_2	L	0.2460	–	0.0116
D64	65%	p_1	N	0.7666	15.649	0.0481
		p_2	L	0.7792	−1.8635e-04	0.0159
	50%	p_1	N	0.3109	81.5	0.0373
		p_2	L	0.4561	−1.2063e-04	0.0116
	35%	p_1	N	0.3092	139.18	0.1393
		p_2	L	0.3052	–	0.0054

the diagrams with experimental results presented in Chapter 3.1. Based on the obtained results, the appropriate linear and nonlinear regression models were created and the p-value of the t-statistic was checked to determine the reproducibility of material removal and surface roughness. When it was smaller than 0.05, the model was assumed as valid at the 5% significance level. A root-mean-square error (RMSE) was used as a measure of the differences between values from experiments and those predicted by models. The experimental results along with the regression equations for the material removal and surface roughness are presented in detail through following sections in Chapter 3.

3. Experiment results and discussion

3.1. Quantitative research

Two series of experiments were conducted for each plating thickness and grain size. The first series was carried out at the pressure $p_1 = 10$ kPa and the second one at $p_2 = 14$ kPa, while other parameters given in Table 1 were constant. The reason for the increase in the surface pressure was the decreasing grinding performance in subsequent tests of the first series. As seen in Fig. 3, abrasive grains located in the thickest plating corresponding to 65% of a nominal diamond size allowed an effective material removal. However, reduction in the surface roughness was relatively small, especially for bigger grain size. A surface roughness parameter Ra slightly decreased from the initial value 1.8 μm to the average one equals to 1.63 μm. In lap-grinding externally applied total force is transmitted to the workpiece through the active abrasive particles and the individual forces depend on the number of active grains. For the lower aerial concentration of bigger grains D107, higher individual forces acted on the abrasive particles as their sum had to be equal to the applied total force [51]. This resulted in larger depth of penetration of the abrasive particles into the workpiece surface and in turn in higher surface roughness. A constant value of Ra = 1.63 μm predicted from a statistically significant linear model (Chapter 3.3) along with the progressive reduction in the material removal rate (Fig. 3 a) indicated that grain dulling was a dominating wear type reducing the grinding performance. For a bigger aerial concentration of smaller grains D64, the number of active particles was higher which led to the decrease of maximum and average forces. This resulted in a lower depth of penetration of the abrasive particles into the workpiece surface and, consequently, in lower material removal, as well as in two times lower surface roughness parameter Ra as compared to bigger D107 grains. The higher pressure applied after 540 s of processing, increased the material removal and decreased gradually the surface roughness. Obtained results indicated that dulling of the grain tips by attrition and fracturing was a dominant wear type for this plating in the second series. Grain dulling reduced the grinding performance and surface roughness. On the other hand, grain fracturing increased the grain density. It improved the surface finish as the individual cutting forces were lower and helped to obtain relatively high material removal as new cutting edges appeared after grain fracturing at the higher pressure. Most likely, the grains were difficult to pull out from the thickest nickel plating due to their smaller initial exposure as a consequence of their deeper immersion in the bond. It resulted in a higher adhesive force due to the larger contact area between grains and the bond, thus protecting grain pullouts. Considering the machining interaction in lapping or polishing as a combination of two-body and three-body wear [52], it can be concluded that two-body abrasion dominated during lap-grinding with the thickest bond when T_b = 65%.

The higher exposure of abrasive grains in the thinner bonds for T_b ratio of 50% and 35% resulted in a lower material removal and in a significant decrease in the surface roughness – Fig. 4 and Fig. 5. This was due to the weaker embedding of grains which allowed their easier removal and the increase in the active grain concentration, hence

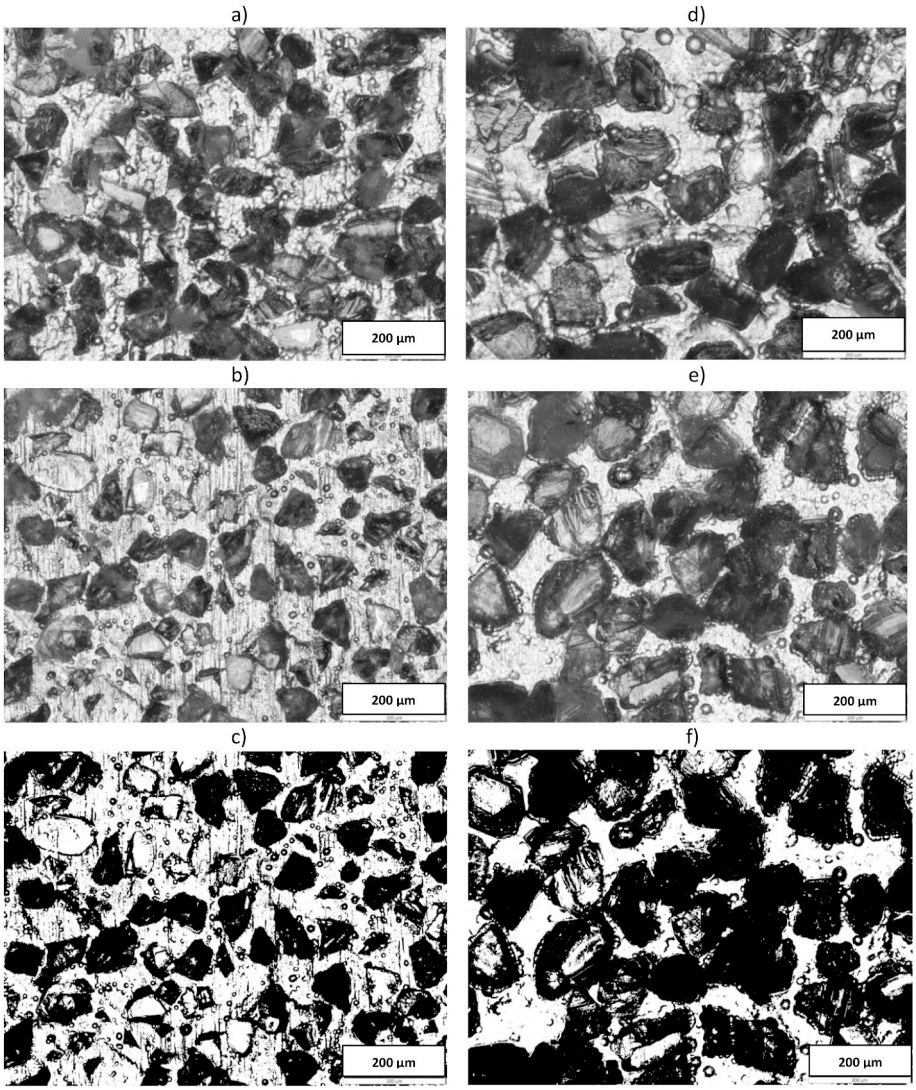

Fig. 6. Microscopic images of non-worn areas of exemplary grinding wheels with D64 diamond grains for $T_b = 65\%$ (a) and $T_b = 35\%$ (b, c) as well as with D107 diamond grains for $T_b = 65\%$ (d) and $T_b = 35\%$ (e, f); images in (c) and (f) are after the binarization of images in (b) and (e), respectively.

reducing the individual forces acting on the active particles. The only exception was a tool with D107 grains more strongly embedded in a nickel bond of an intermediate height ($T_b = 50\%$) but not as strongly as in the thickest bond ($T_b = 65\%$). Due to that, the surface finish gradually improved but a parameter Ra did not fall below Ra = 1 µm (Fig. 4). The material removal at $t_p = 540$ s was bigger for the thinnest plating characterized by the highest initial grain protrusion. The higher pressure applied in the second series after $t_p = 540$ s increased the material removal for $T_b = 50\%$ and grain size D107, however, it significantly limited the material cutting process for $T_b = 35\%$ and both D107 and D64 sizes, what is clearly seen in Fig. 4 a and Fig. 5 a, respectively. Due to the minimal material loss and the noticeable intensive tool wear for $T_b = 35\%$, the experiments with D64 grains were discontinued after the test number 10. As the observations showed, the wheel wear was characterized mainly by the pullout and fracture of the weakly held grains immersed in the thinnest bond. The lowest immersion in the bond as well as the highest exposure of abrasive grains facilitated their removal and crushing into smaller pieces. The increase in the active grain density reduced the individual forces acting on the active particles. Smaller particles and lower forces were responsible for the intensive decrease in the workpiece surface roughness to the steady state values for both grain sizes (Fig. 5 b). This also applies to the values determined from the models. Fracturing and crushing of the abrasive grains resulted in an abrasive slurry similar to that used in conventional lapping. This may suggest the process transition from grinding treated as two-body abrasion for the thickest bond ($T_b = 65\%$) to conventional lapping treated as three-body abrasion for the thinnest bond ($T_b = 35\%$). For the intermediate bond thickness ($T_b = 50\%$) the surface finish differed considerably for both grain sizes (Fig. 4 b). The course of machining and obtained values of Ra parameter indicated that two-body abrasion was dominating for D107 grains and three-body abrasion for D64 grains.

3.2. Regression equations for determining the material removal

As expected, the material removal rate showed the decreasing tendency during all tests. The cumulative material loss increased towards a maximum value with gradual wear of the tool. Therefore, the relationship between the material removal and the processing time was approximated considering the tendencies and shapes of the experimentally determined curves by asymptotic mathematical functions, as suggested by [53]. Two models of the material removal formulated as functions of a processing time were considered:

$$\text{model A}: \qquad H_a(t_p) = b_{A1} \,/\, (1 \,/\, t_p + b_{A2}), \qquad t_p > 0, \tag{2}$$

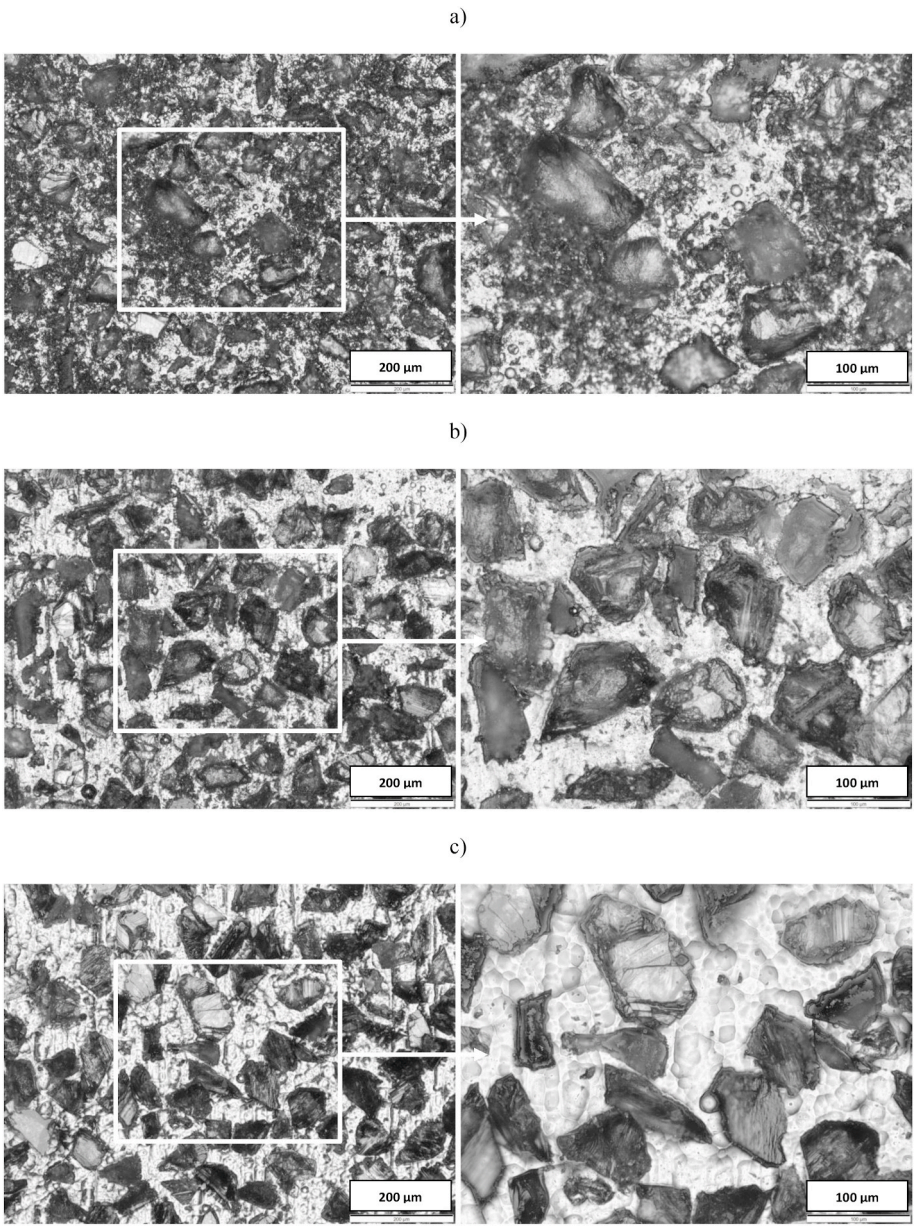

Fig. 7. Worn areas of grinding wheels after all lap-grinding experiments with D64 diamond grains and the different thickness of a nickel plating: a) $T_b = 35\%$, b) $T_b = 50\%$, c) $T_b = 65\%$.

$$\text{model B}: \qquad H_B(t_p) = b_{B1} \cdot \exp(b_{B2} / t_p), \qquad t_p > 0, \tag{3}$$

where H_A and H_B are the material removals (height reduction) in millimeters, t_p is the processing time in seconds and b_1, b_2 are model coefficients determined on the basis of experimental data.

Horizontal asymptotes of Equation (2) and Equation (3) are expressed as:

$$\text{for model A:} \qquad y_A = b_{A1}/b_{A2}\,, \tag{4}$$

$$\text{for model B:} \qquad y_B = b_{B1}. \tag{5}$$

Horizontal asymptotes of the proposed nonlinear regression models can be assumed as the maximum theoretical height reduction that may occur during single-sided lap-grinding under given technological parameters. The software Matlab by MATHWORKS, Natick, Massachusetts, USA, was used to process the data and perform the curve fitting. For the created nonlinear models expressed by Equation (2) and Equation (3), the *p*-value of the *t*-statistic was checked. If it was smaller than 0.05, the model was assumed as valid at the 5% significance level. In addition, a root-mean-square error (RMSE) was used as a measure of the differences between the experimental values and those predicted from models. As both models were statistically significant for all tools, the lower value of RMSE determined the model selection. The values of model coefficients evaluated for all tools used in the first series of experiments during a processing time $0 < t_p \leq 540$ s, are listed in Table 2. As seen in Table 2, model A enabled more accurate curve fitting for the thickest plating - Fig. 3 a, whereas, model B for the thinnest one - Fig. 5 a. For the intermediate bond thickness, model A was selected for bigger D107 grains, while model B for smaller D64 grains – Fig. 4 a. Obtained results indicated that model A is more suitable for strongly held grains immersed in the thickest bond ($T_b = 65\%$) and the model B for weakly held grains immersed in the thinnest bond ($T_b = 35\%$). In addition, model A corresponds to two-body - and model B to three-body abrasion, identified as the dominant processes for the relevant experiments.

Due to the fact that in the second series of experiments the nominal

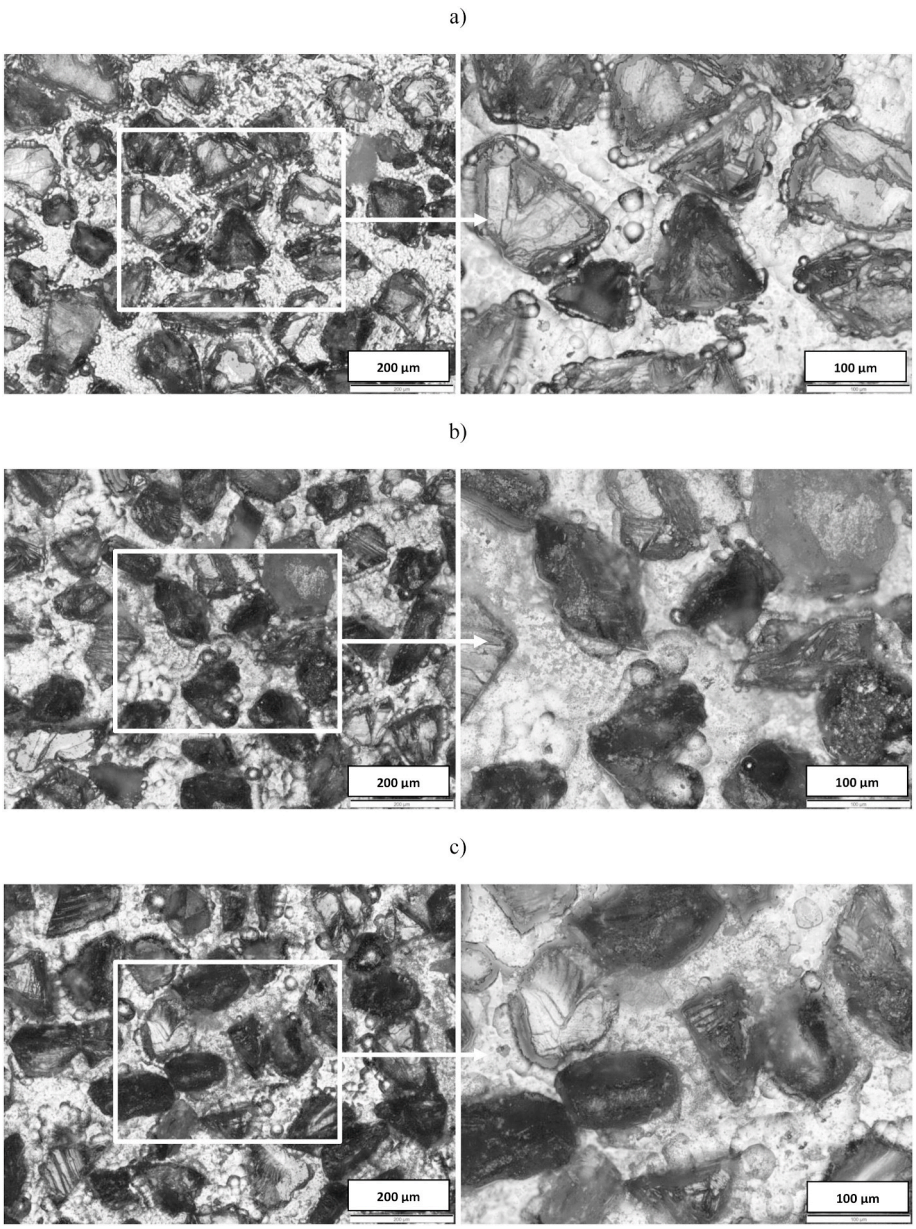

Fig. 8. Worn areas of grinding wheels after all lap-grinding experiments with D107 diamond grains and the different thickness of a nickel bond: a) $T_b = 35\%$, b) $T_b = 50\%$, c) $T_b = 65\%$.

pressure was increased, the models described by Equation 2 and Equation 3 were modified according to the Preston's equation. It is based on the experimental observation that the removal rate is proportional to the nominal applied pressure and the relative velocity between the tool and the workpiece. It was effectively used in the analysis of the material removal in CMP [54] and for modelling the tool wear during lapping [55]. Preston's equation for the material removal rate can be written as:

$$\frac{\Delta H}{\Delta t} = \mathrm{k}\cdot\mathrm{p}\cdot\mathrm{v} \tag{6}$$

where k is termed as the Preston constant, p is the nominal pressure and v is the relative velocity.

When k and v are constant in a specified time interval Δt, the nominal pressure change from p_1 to p_2 defines the relationship between the material removals as:

$$\Delta H_2 = \frac{\mathrm{p}_2}{\mathrm{P}_1}\cdot\Delta H_1 \tag{7}$$

Taking into account the dependence resulting from Equation (7), the material removal during machining with the pressure change (an increase or a decrease) will be:

$$H^{'}(t_p) = H(t_{p1}) + \frac{P_2}{P_1}[H(t_p)], \quad t_p > 0 \wedge t_p > t_{p1} \tag{8}$$

where: H is the material removal described by Equation (2) or Equation (3), t_{p1} is the time of the pressure change from p_1 to p_2.

Results predicted by Equation (8) after 540 s of processing ($t_{p1} = 540$ s), when the nominal applied pressure was changed from $p_1 = 10$ kPa to $p_2 = 14$ kPa, are presented in Fig. 3 a, Fig. 4 a and Fig. 5 a, as models A′ and B′, correspondingly to the initial models A and B. The higher pressure applied in the second series after $t_{p1} = 540$ s increased the material removal for $T_b = 65\%$ and both grain sizes as well as for $T_b = 50\%$ and grain size D107. It was also predicted by model A′ as seen in Fig. 3 a and Fig. 4 a. For $T_b = 35\%$, experimental data after 540 s of processing were much below the removal rates predicted by model B' and even by the model B. This confirmed the intensive wear and the shortest life of a tool

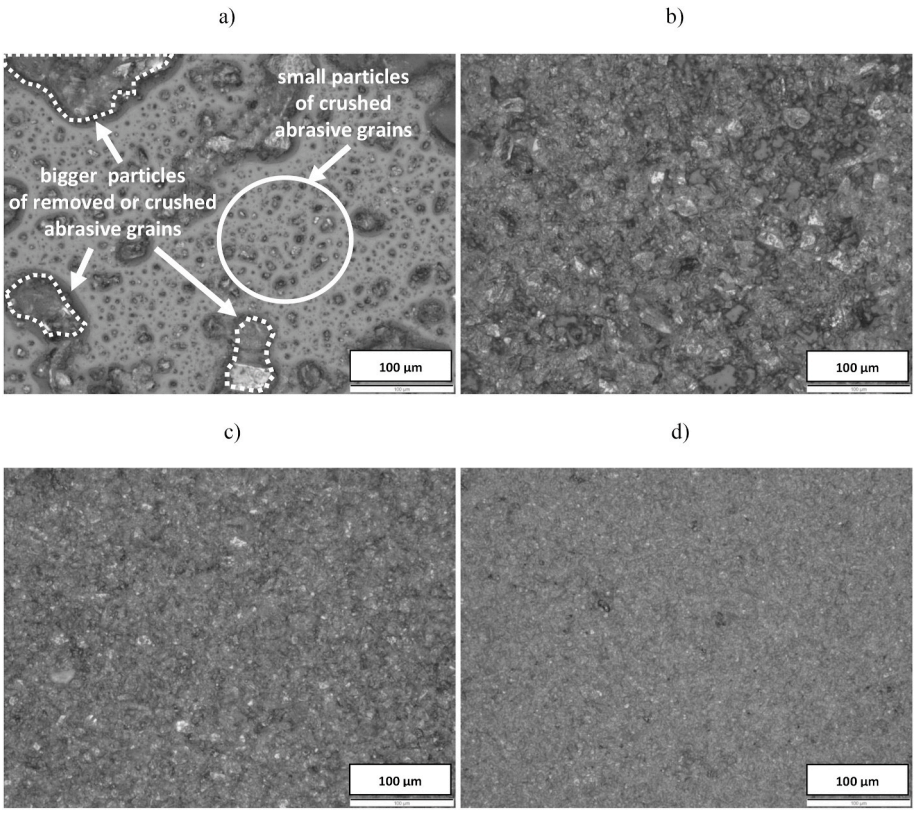

Fig. 9. Abrasive slurry taken from the active surface of the tool with D64 grains and the plating ratio $T_b = 35\%$ after a processing time t_p of: a) 90 s, b) 180 s, c) 270 s, d) 360 s.

with the thinnest plating – Fig. 5 a.

3.3. Regression equations for determining the surface roughness

Similarly as for the material removal, the relationship between the surface roughness and the processing time was approximated, taking into account the trends in changes in obtained experimental results. Two models of a surface roughness parameter Ra formulated as functions of processing time t_p were analyzed:

$$\text{linear model L:} \quad Ra_L(t_p) = b_{L1} + b_{L2} \cdot t_p, \qquad t_p > 0, \tag{9}$$

$$\text{nonlinear model N:} \quad Ra_N(t_p) = b_{N1} \cdot exp\left(b_{N2}/t_p\right), \qquad t_p > 0 \tag{10}$$

where Ra_L and Ra_N are the values of the theoretical Ra surface roughness parameter in micrometers, t_p is the processing time in seconds, b_1 and b_2 are model coefficients determined on the basis of experimental data.

Selected models with the values of model coefficients are presented in Table 3. In the first step of the analysis, a linear model with both coefficients b_{L1} and b_{L2} was analyzed and the p-value of the t-statistic was checked. If it was smaller than 0.05 for both coefficients, the model was assumed as valid at the 5% significance level. When the p-value of the t-statistic for b_{L2} was greater than 0.05, the linear model with only one coefficient b_{L1} was analyzed. When the p-value of the t-statistic for b_{L1} again was greater than 0.05 than the nonlinear model was created and tested.

The nonlinear models statistically significant at the 5% significance level enabled accurate curve fitting to the surface roughness data for most tools during lap-grinding under the nominal pressure $p_1 = 10$ kPa and for the processing time $t_p \leq 540$ s – Table 3. The only exception was the tool with the thickest plating ($T_b = 65\%$) and D107 diamond grains for which a constant linear model was adopted. The nonlinear models created for the tools with the thinnest plating ($T_b = 35\%$) had the highest values of RMSE. These tools with D107 and D64 grains were also characterized by the biggest reduction in the workpiece surface roughness – Fig. 5 b. A horizontal asymptote ($y_N = b_{N1}$) of a nonlinear model can be assumed as the theoretical surface roughness parameter Ra to be obtained during single-sided lap-grinding under given technological parameters. Even the nominal pressure change from $p_1 = 10$ kPa to $p_2 = 14$ kPa at a time $t_{p1} = 540$ s, allowed obtaining the values of Ra parameter which were relatively close (usually below) to the theoretical values calculated from nonlinear models extrapolated beyond t_{p1}. Nevertheless, the statistically significant linear model was assumed for all tools during processing under the higher pressure $p_2 = 14$ kPa – Table 3. The constant value of Ra was predicted by a linear model created for the tools with the thinnest plating ($T_b = 35\%$). These tools were characterized by the lowest material removal rate and an intensive wear after $t_{p1} = 540$ s (Fig. 5).

3.4. Qualitative research

The decrease in surface roughness and material removal rate in time can be explained qualitatively, assuming that in lapping of brittle materials fracture processes play a more dominant role than plastic flow mechanism [51,56]. For a given nominal pressure and grain concentration, the grains' crushing and fracturing reduce their exposure H_p (Fig. 2 b). Due to that, the number of active particles seems to increase, but the maximum and average loads per active particle decrease. As a result, a more shallow indentation of the abrasive particles into the workpiece occurs, causing lateral cracks at smaller depths. Consequently, smaller particles are removed from the ceramic workpiece, hence improving the surface finish and reducing the removal rate. As the number of active particles decreases when the particle size is bigger, Ra would be expected to increase for bigger grains D107. The above

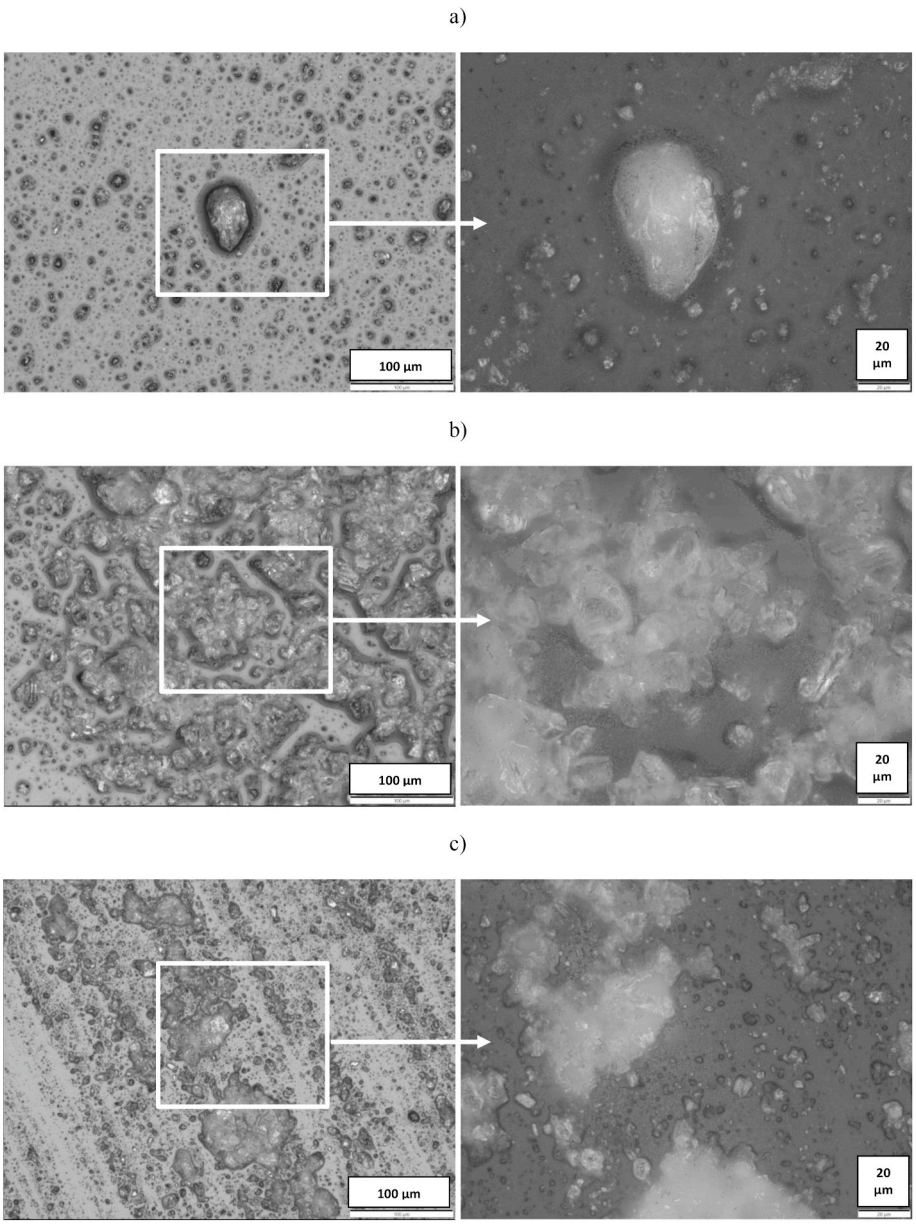

Fig. 10. Abrasive slurry taken after a processing time $t_p = 90$ s from the active surface of the tool with D64 grains and the plating ratio: a) $T_b = 35\%$, b) $T_b = 50\%$, c) $T_b = 65\%$.

inference was confirmed by experimental and computational results presented in Chapter 3.1, as well as in Chapter 3.2. and Chapter 3.3, respectively. Moreover, the gradual reduction in the lap-grinding efficiency limited the tool life of electroplated wheels which were subject to wearing down. The qualitative research allowed to reveal information on the wear of the active surface of the grinding wheels. For this purpose, the OLYMPUS BX51 microscope with dedicated OLYMPUS Stream Motion software was used to observe the active surface of the grinding wheels and the resulting slurry. Fig. 6 presents the images of non-worn areas of exemplary grinding wheels with grains of different size and height exposure. There is a visible difference in the aerial concentration of abrasive grains determined by the examination of microscopic images to: $C_{64} = 130$ mm^{-2} for smaller D64 grains and $C_{107} = 70$ mm^{-2} for larger D107 grains.

Grinding wheels with larger abrasive D107 grains were characterized by smaller free space between grains. It was confirmed by the image binarization process, consisting in determining the percentage ratio of the number of white pixels representing the free space between abrasive grains to the total number of pixels for each of the analyzed images – Fig. 6 c and Fig. 6 f. Estimated values for the tools with D64 and D107 grains were ~45% and ~30%, respectively. This indicated different sizes of areas of free space between grains, although the light reflections and the initial image brightness affected obtained results. Since the initial surface concentration of the abrasive grains was the same for different bond thicknesses, the images showed no significant quantitative or qualitative differences for $T_b = 35\%$ and $T_b = 65\%$.

The differences are visible, however, in the images of grinding wheels fragments after all tests had been carried out – Fig. 7 and Fig. 8. These figures show a significant influence of the depth of embedding the abrasive grains in the bond layer on the wear of the active tool surface. The wear was the result of the grains pullout, crushing and blunting, as was also observed in Ref. [38,43]. Ripping the D64 grains from the thinnest nickel bond significantly reduced their initial aerial concentration and consequently increased the free space with small particles of crushed grains – Fig. 7 a. This increased the number of active grains consisted of originally embedded grains as well as particles of fractured

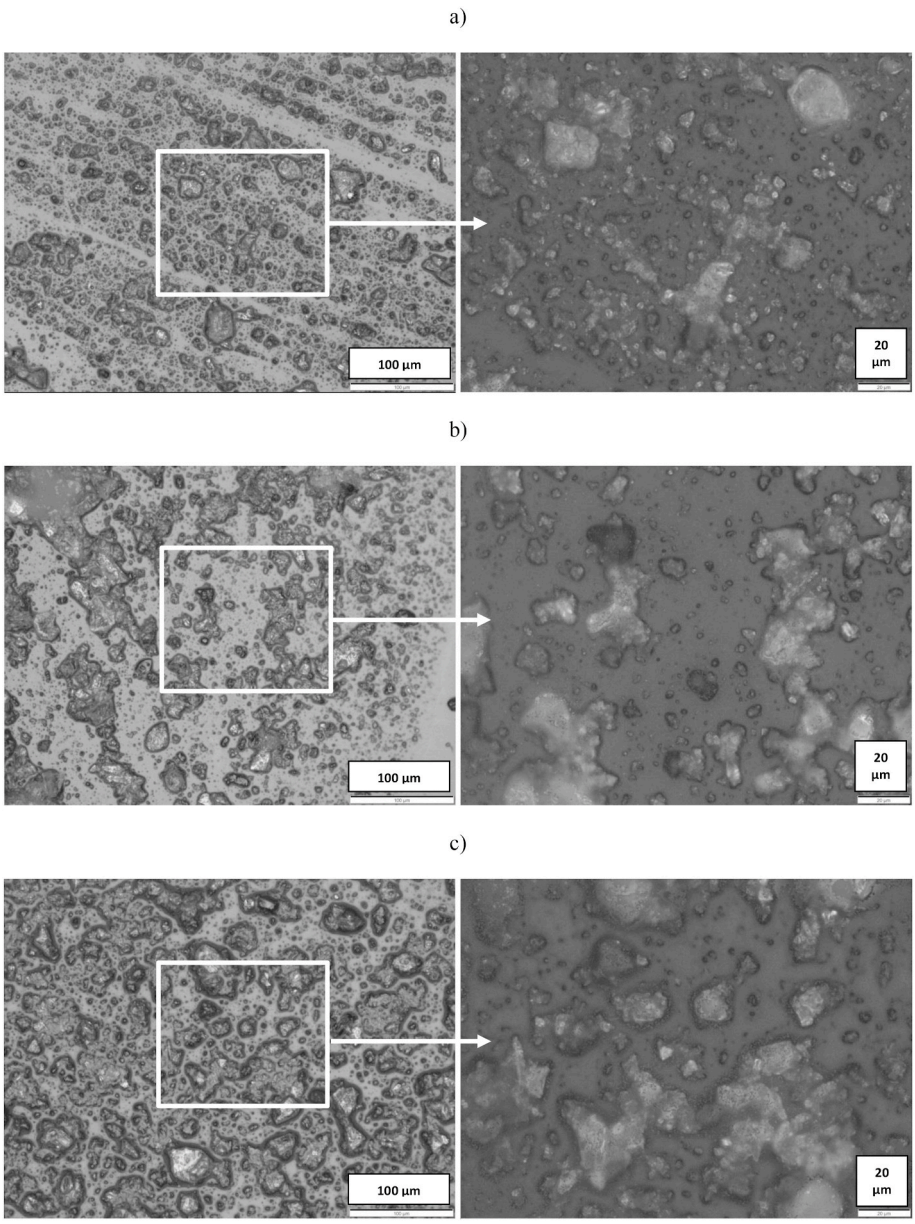

Fig. 11. Abrasive slurry taken after a processing time $t_p = 90$ s from the active surface of the tool with D107 grains and the plating ratio: a) $T_b = 35\%$, b) $T_b = 50\%$, c) $T_b = 65\%$.

grains. For other nickel bond thicknesses characterized by the plating ratio $T_b = 50\%$ and $T_b = 65\%$, the dominating form of the wear was the grains dulling and fracturing with a very few removals from the binder. For the thicker nickel bond, the number of grits of crushed abrasive grains is lower and the free space between grains less contaminated by abrasive or ceramic particles - Fig. 7 b, c. As seen in Fig. 8, the bond thickness had a smaller effect on the removal of D107 grains immersed in the plating. Most likely, that was due to the larger contact area between D107 grains and the bond, which resulted in an adhesive force greater than in the case of smaller D64 grains.

The observed tendencies in the wear of the active surface of grinding wheels were confirmed during the analysis of microscopic images of the abrasive slurry. The slurry was collected from the active surface of the tool directly after each subsequent test. Bigger differences in the slurry composition were clearly seen at the initial stage of machining, as demonstrated for the first four tests with D64 grains and the plating ratio $T_b = 35\%$ - Fig. 9. Fragments of particles of various sizes, bigger ones removed from the bond and smaller ones of crushed abrasive grains, were visible in the obtained slurry after a processing time $t_p = 90$ s. Due to the presence of larger abrasive particles, the surface roughness was reduced only slightly after the first test with D64 grains – Fig. 5 b. As there was no additional abrasive delivered into the working zone, apart from grains immersed in a layer of bond, the visible fragments of the abrasive grains must come from the electroplating tool. Comparing to the scale, most of the particles are much smaller than D64 diamond grains with the average size of $d_g = 64$ µm. In addition, and due to the grain pullout, Fig. 7 a shows fewer grains in the worn active tool surface with the thinnest bond ($T_b = 35\%$) than in the tool with thicker bonds (Fig. 7 b, c). This confirms that the bigger particles visible in Fig. 9 a are grains removed from the thinnest bond during the first test. Smaller particles were the result of grain crushing. During subsequent tests, the abrasive particles were further crushed and mixed with those of the removed workpiece material which resulted in obtaining a uniform abrasive slurry - Fig. 9 d. This caused a significant reduction of the workpiece surface roughness until a certain value was reached, after which the roughness remained constant or changed only slightly – Fig. 4

b and Fig. 5 b.

Fragments of the resulting abrasive slurry after the first test using tools with D64 and D107 grains as well as different bond thickness are presented in Fig. 10 and Fig. 11, respectively. Abrasive particles in the slurry confirmed grinding wheel wear due to whole grains being removed from the galvanic bond or particles of still embedded grains being chipped off. Similarly to Fig. 9 a, larger fragments of abrasive particles can be observed after machining with grinding wheels with the thinnest plating, from which the grains were more easily removed – Fig. 10 a and Fig. 11 a. Smaller particles chipped from more strongly bonded abrasive grains formed characteristic conglomerates that also included ceramic particles removed from the workpiece surface – Fig. 10 b, c and Fig. 11 b, c. More strongly bonded abrasive grains in thicker plating more effectively facilitated the removal of particles from the workpiece, which were visible in the suspension that formed on the active surface of the grinding wheel. Therefore, deeper grain embedding resulted in the higher machining efficiency – Fig. 3 a. After consecutive tests, the abrasive slurry was characterized by an increasingly uniform structure due to finer abrasive particles - higher grain crushing, and smaller particles of the workpiece.

4. Conclusions

The size of the abrasive grains and the depth of their embedding in the nickel bond had a significant influence on the wear of diamond electroplated grinding wheels as well as on the technological effects. Main conclusions from the performed research could be drawn as follows:

- Highest efficiency was obtained for the thickest layer of a nickel bond characterized by the plating thickness $T_b = 65\%$. Abrasive grains more immersed in the plating were difficult to pull out from the active surface of the grinding wheel. As a result, the dulling of the grain tips by attrition and fracturing was observed as a dominant wear type for this plating.
- Wheel wear was accompanied by a decrease in the material removal and in the surface roughness of machined samples which was the lowest for the thinnest nickel bond characterized by the plating ratio $T_b = 35\%$. The wheel wear was characterized mainly by the pullout and fracture of the weakly held grains immersed in the thinnest bond.
- Fracturing and crushing of the abrasive grains immersed in the thinnest plating resulted in an abrasive slurry similar to that used in conventional lapping. As confirmed by the microscopic observations of worn grinding wheels and the slurry, this led to the process transition from grinding treated as two-body abrasion to conventional lapping treated as three-body abrasion.
- The relationship between the material removal and the processing time was approximated by asymptotic mathematical functions. One of the advantages of the proposed models, called A and B, is that the maximum theoretical material removal can be calculated directly from the functions coefficients using proposed equations.
- Empirical and simulation results indicated that the model A is more suitable for strongly held grains immersed in the thickest bond ($T_b = 65\%$) and the model B for weakly held grains immersed in the thinnest bond ($T_b = 35\%$). As both models were statistically significant, the lower value of RMSE determined the model selection.
- The empirical models were modified according to the Preston's equation when the unit pressure increased. This allowed the formulation of the general equation describing the material removal during machining with an increase or a decrease in the nominal pressure.
- The regression models enabled also accurate curve fitting to the surface roughness data. A horizontal asymptote of a proposed nonlinear model can be assumed as a theoretical surface roughness parameter Ra to be obtained during single-sided lap-grinding under given technological parameters.

Declaration of competing interest

The authors declare that they have no known competing financial interests or personal relationships that could have appeared to influence the work reported in this paper.

Acknowledgements

Computations carried out with the use of the software and computers from Academic Computer Centre in Gdańsk, Poland - TASK (http://www.task.gda.pl). Experiments were partially financed by Polish budget funds for science as a research project N N503 157638. Special thanks to Mr. Steve Lionas from Diamondback Abrasive (https://www.diamondbackabrasive.com/) for manufacturing and providing electroplated diamond wheels. Authors would like to thank Dr. Agata Sommer from the Faculty of Chemisty, Gdańsk University of Technology for the pH measurements.

Appendix A. Supplementary data

Supplementary data to this article can be found online at https://doi.org/10.1016/j.wear.2020.203461.

References

[1] K. Żak, W. Grzesik, Metrological aspects of surface topographies produced by different machining operations regarding their potential functionality, Metrol. Meas. Syst. 24 (2) (2017) 325–335.
[2] F. Molaiekiya, M. Aramesh, S.C. Veldhuis, Chip formation and tribological behavior in high-speed milling of IN718 with ceramic tools, Wear 446 (2020), 203191.
[3] E. Medvedovski, Wear-resistant engineering ceramics, Wear 249 (9) (2001) 821–828.
[4] P. Pawar, R. Ballav, A. Kumar, An overview of machining process of alumina and alumina ceramic composites, Manuf. Sci. Technol. 3 (1) (2015) 10–15.
[5] K. Poser, K.H. Zum Gahr, J. Schneider, Development of Al2O3 based ceramics for dry friction systems, Wear 259 (1–6) (2005) 529–538.
[6] C.W. Chang, C.P. Kuo, Evaluation of surface roughness in laser-assisted machining of aluminum oxide ceramics with Taguchi method, Int. J. Mach. Tool Manufact. 47 (1) (2007) 141–147.
[7] Y. Liang, S.P. Dutta, Application trend in advanced ceramic technologies, Technovation 21 (1) (2001) 61–65.
[8] T.G. Bifano, T.A. Dow, R.O. Scattergood, Ductile-regime grinding: a new technology for machining brittle materials, J. eng. ind. 113 (2) (1991) 184–189.
[9] S. Malkin, C. Guo, Thermal analysis of grinding, CIRP Annals 56 (2) (2007) 760–782.
[10] Z.J. Pei, A. Strasbaugh, Fine grinding of silicon wafers, Int. J. Mach. Tool Manufact. 41 (5) (2001) 659–672.
[11] M. Szkodo, K. Chodnicka-Wszelak, M. Deja, A. Stanisławska, M. Bartmański, The influence of the depth of cut in single-pass grinding on the microstructure and properties of the C45 steel surface layer, Materials 13 (5) (2020), 1040.
[12] C. Park, H. Kim, S. Lee, H. Jeong, The influence of abrasive size on high-pressure chemical mechanical polishing of sapphire wafer, Int. J. Precision Eng. Manuf.-Green Tech. 2 (2) (2015) 157–162.
[13] H. Singh, P.K. Jain, Lapping, in: V.K. Jain (Ed.), *Nanofinishing Science and Technology*: Basic and Advanced Finishing and Polishing Processes, CRC Press, 2016, pp. 79–92.
[14] T. Shibata, B. Golman, K. Shinohara, M. Otani, T. Uchiyama, Profile analysis of surfaces lapped with diamond particles of several shapes, Wear 254 (7–8) (2003) 742–748.
[15] L.S. Deshpande, S. Raman, O. Sunanta, C. Agbaraji, Observations in the flat lapping of stainless steel and bronze, Wear 265 (1–2) (2008) 105–116.
[16] A. Choudhary, A. Naskar, S. Paul, Effect of minimum quantity lubrication on surface integrity in high-speed grinding of sintered alumina using single layer diamond grinding wheel, Ceram. Int. 44 (14) (2018) 17013–17021.
[17] M. Emami, M.H. Sadeghi, A.A.D. Sarhan, F. Hasani, Investigating the minimum quantity lubrication in grinding of Al_2O_3 engineering ceramic, J. Clean. Prod. 66 (2014) 632–643.
[18] B. Li, J. Ni, J. Yang, S.Y. Liang, Study on high-speed grinding mechanisms for quality and process efficiency, Int. J. Adv. Manuf. Technol. 70 (5–8) (2014) 813–819.
[19] K. Ramesh, S.H. Yeo, S. Gowri, L. Zhou, Experimental evaluation of super high-speed grinding of advanced ceramics, Int. J. Adv. Manuf. Technol. 17 (2) (2001) 87–92.

[20] Y. Liu, B. Li, C. Wu, Y. Zheng, Simulation-based evaluation of surface micro-cracks and fracture toughness in high-speed grinding of silicon carbide ceramics, Int. J. Adv. Manuf. Technol. 86 (1–4) (2016) 799–808.
[21] X. Zhu, C. Chung, C.S. Korach, I. Kao, Experimental study and modeling of the effect of mixed size abrasive grits on surface topology and removal rate in wafer lapping, Wear 305 (1–2) (2013) 14–22.
[22] M. Deja, Simulation model for the shape error estimation during machining with flat lapping kinematics, in: ASME 2010 International Manufacturing Science and Engineering Conference, vol. 1, American Society of Mechanical Engineers Digital Collection, 2010, pp. 291–299, https://doi.org/10.1115/MSEC2010-34262.
[23] A. Barylski, M. Deja, Wear of a tool in double-disk lapping of silicon wafers, in: ASME 2010 International Manufacturing Science and Engineering Conference, vol. 1, American Society of Mechanical Engineers Digital Collection, 2010, pp. 301–307, https://doi.org/10.1115/MSEC2010-34323.
[24] J.F.G.D. Oliveira, E.J.D. Silva, C. Guo, F. Hashimoto, Industrial challenges in grinding, CIRP annals 58 (2) (2009) 663–680.
[25] J.Y. Shen, X.P. Xu, B. Lin, Y.S. Xu, Lap-grinding of Al_2O_3 ceramics assisted by water-jet dressing metal bond diamond wheel, Key Eng. Mater. 202–203 (2001) 171–176. https://doi.org/10.4028/www.scientific.net/kem.202-203.171.
[26] A.B. Khoshaim, Z. Xu, I.D. Marinescu, ELID grinding with lapping kinematics, in: Handbook of Ceramics Grinding and Polishing, William Andrew Publishing, 2015, pp. 394–448.
[27] Z. Wang, F. Niu, Y. Zhu, J. Li, J. Wang, Comparison of lapping performance between fixed agglomerated diamond pad and fixed single crystal diamond pad, Wear 432–433 (2019), 202963.
[28] H.M. Kim, R. Manivannan, D.J. Moon, H. Xiong, J.G. Park, Evaluation of double sided lapping using a fixed abrasive pad for sapphire substrates, Wear 302 (1–2) (2013) 1340–1344.
[29] M. Deja, M. List, L. Lichtschlag, E. Uhlmann, Thermal and technological aspects of double face grinding of Al_2O_3 ceramic materials, Ceram. Int. 45 (15) (2019) 19489–19495, https://doi.org/10.1016/j.ceramint.2019.06.206.
[30] E. Uhlmann, M. List, M. Patraschkov, G. Trachta, A new process design for manufacturing sapphire wafers, Precis. Eng. 53 (2018) 146–150.
[31] H.M. Kim, G.H. Park, Y.G. Seo, D.J. Moon, B.J. Cho, J.G. Park, Comparison between sapphire lapping processes using 2-body and 3-body modes as a function of diamond abrasive size, Wear 332–333 (2015) 794–799.
[32] A. Barylski, M. Deja, Microgrinding of flat surfaces on single-disc lapping machine, Int. J. Mach. Mach. Mater. 5 (2–3) (2009) 245–267.
[33] E. Uhlmann, T. Hoghé, Wear reduction at double face grinding with planetary kinematics, J. Inst. Eng. Prod. 6 (3) (2012) 237–242.
[34] M. Deja, Correlation between shape errors in flat grinding, Journal of Vibroengineering 14 (2) (2012) 520–527.
[35] B.J. Cho, H.M. Kim, R. Manivannan, D.J. Moon, J.G. Park, On the mechanism of material removal by fixed abrasive lapping of various glass substrates, Wear 302 (1–2) (2013) 1334–1339.
[36] A. Barylski, M. Deja, Finishing of ceramics in a single-disk lapping machine configuration, in: Solid State Phenomena, vol. 165, Trans Tech Publications Ltd, 2010, pp. 237–243.
[37] L.E.A. Sanchez, N.X. Jun, A.A. Fiocchi, Surface finishing of flat pieces when submitted to lapping kinematics on abrasive disc dressed under several overlap factors, Precis. Eng. 35 (2) (2011) 355–363.
[38] M. Deja, Single-side grinding with the use of electroplated tools, in Polish, Mech 88 (8–9CD1) (2015) 84–89.
[39] R.P. Upadhyaya, S. Malkin, Thermal aspects of grinding with electroplated CBN wheels, J. Manuf. Sci. Eng. 126 (1) (2004) 107–114.
[40] M.F. Ismail, K. Yanagi, H. Isobe, Characterization of geometrical properties of electroplated diamond tools and estimation of its grinding performance, Wear 271 (3–4) (2011) 559–564.
[41] D. Bhaduri, R. Kumar, A.K. Jain, A.K. Chattopadhyay, On tribological behaviour and application of TiN and MoS2-Ti composite coating for enhancing performance of monolayer cBN grinding wheel, Wear 268 (9–10) (2010) 1053–1065.
[42] Z. Shi, S. Malkin, An investigation of grinding with electroplated CBN wheels, CIRP Ann. - Manuf. Technol. 52 (1) (2003) 267–270.
[43] Z. Shi, S. Malkin, Wear of electroplated CBN grinding wheels, J. Manuf. Sci. Eng. 128 (1) (2006) 110–118.
[44] R.P. Upadhyaya, J.H. Fiecoat, Factors affecting grinding performance with electroplated CBN wheels, CIRP Ann. - Manuf. Technol. 56 (1) (2007) 339–342.
[45] M. Deja, Estimation of the active surface condition of the electroplated tool in grinding with lapping kinematics, in Polish, Inżynieria Maszyn 18 (2) (2013) 45–54.
[46] M. Deja, Wear of electroplated tools used for flat grinding of ceramics, in: Solid State Phenomena, vol. 199, Trans Tech Publications Ltd, 2013, pp. 633–638.
[47] A. Barylski, M. Deja, Influence of flat lapping kinematics on machinability of ceramics, in: Solid State Phenomena, vol. 199, Trans Tech Publications Ltd, 2013, pp. 615–620.
[48] M. Deja, Vertical vibration reduction and audible sound analysis in surface grinding with electroplated tools, J. Measure. Eng. 2 (2) (2014) 80–85.
[49] S. Novak, M. Kalin, The effect of pH on the wear of water-lubricated alumina and zirconia ceramics, Tribol. Lett. 17 (4) (2004) 727–732.
[50] A.J. Gant, M.G. Gee, Sliding wear corrosion of ceramics, Wear 267 (1–4) (2009) 599–607.
[51] V.H. Bulsara, Y. Ahn, S. Chandrasekar, T.N. Farris, Polishing and lapping temperatures, J. Tribol. 119 (1) (1997) 163–170.
[52] J.H. Horng, Y.R. Jeng, C.L. Chen, A model for temperature rise of polishing process considering effects of polishing pad and abrasive, J. Tribol. 126 (3) (2004) 422–429.
[53] M. Korzyński, „Methodology of the Experiment. Planning, Implementation and Statistical Analysis of the Results of Technological Experiments", 2018, Publisher House: Wydawnictwo WNT, Polish, 2013, 277.
[54] L. Guo, R.S. Subramanian, Mechanical removal in CMP of copper using alumina abrasives, J. Electrochem. Soc. 151 (2) (2004) G104–G108.
[55] A. Barylski, N. Piotrowski, Non-conventional approach in single-sided lapping process: kinematic analysis and parameters optimization, Int. J. Adv. Manuf. Technol. 100 (1–4) (2019) 589–598.
[56] R. Chauhan, Y. Ahn, S. Chandrasekar, T.N. Farris, Role of indentation fracture in free abrasive machining of ceramics, Wear 162 –164 (1993) 246–257. Part A.